Diamond & Related Materials 92 (2019) 248–252

Contents lists available at ScienceDirect

Diamond & Related Materials

journal homepage: www.elsevier.com/locate/diamond

Non-contact polishing of single crystal diamond by ion beam etching

Sichen Mi*, Adrien Toros, Teodoro Graziosi, Niels Quack*

École Polytechnique Fédérale de Lausanne (EPFL), Lausanne CH-1015, Switzerland

ARTICLE INFO

Keywords:
Single crystal diamond
Polishing
Ion beam etching
Precision engineering
Sub-surface damage

ABSTRACT

We propose a non-contact surface finishing method for brittle substrates by ion beam etching and we experimentally demonstrate polishing of (100) single crystal diamond surface. We model and simulate the polishing process, and verify the results experimentally by monitoring individual defects during the surface treatment. Rapid flattening of scratches and digs, as typically present on brittle substrates after mechanical polishing, is observed: trench depth is typically removed by 95% in less than 30 min. The polishing method relies on physical bombardment of the substrate surface with accelerated inert gas ions, rendering it highly versatile and applicable to a wide variety of materials.

1. Introduction

Single crystal diamond (SCD) has for long drawn interest in fundamental and engineering research, owing to its outstanding material properties [1], such as the highest thermal conductivity and mechanical hardness of any known bulk material, ultra-wide optical transparency, as well as extraordinary resistance to various chemicals. In addition, recently revealed quantum characteristics of diamond lattice defects have made it particularly appealing for atomic level sensing [2] and quantum information processing [3]. Current technology in chemical vapour deposition (CVD) has led to the demonstration of high-quality synthetic SCD [4], and polished SCD plates of dozens of square millimeters in size and hundreds of microns in thickness have become commercially available [5,6], suggesting that SCD may serve as an ideal material platform for large-scale nanophotonics applications.

However, the mechanical hardness and chemical inertness of diamond make it extremely difficult to process. Various techniques have been developed to achieve substrate preparation and meanwhile allow preserving excellent material quality [7,8]. Among the traditional processing methods, mechanical polishing, studied over centuries [9], continues to serve as the principal substrate preparation method, and is still being actively investigated [10,11] to improve device performance [12].

Recently, several non-contact polishing methods have been shown to be useful for smoothening the polishing lines without inducing further damages, including dressed-photon-phonon etching [13], reactive ion etching (RIE) with specific recipes [14,4], and ion beam etching (IBE) with incidence angle smaller than 45° [15, 16]. However they are not suitable for removing deep scratches. Consequently, a time-consuming fine polishing step remains the prevalent surface preparation method [12]. With the requirements for precision engineering and miniaturization of optoelectronic devices, developing efficient polishing techniques for hard and brittle materials [17-19] is of great importance and practical value. In this report, we present a non-contact surface polishing method using IBE with simultaneous sample rotation, which is fast and circumvents the difficulties associated with the surface preparation by traditional fine polishing methods, such as polishing-induced subsurface damages [9].

2. Material and methods

2.1. As-received diamond substrate

An atomic force microscope (AFM) measurement of a typical mechanically polished (100) surface of a SCD substrate is shown in Fig. 1. Abundant scratches and polishing lines are found on the as-received sample purchased from Element Six [6] (general grade, 2.6 mm × 2.6 mm × 0.3 mm). The AFM measurement reveals regions with very smooth surface (about 2–3 Å surface roughness Ra over 500 nm × 500 nm area), where shallow polishing lines are present, as can be seen on the top left part of Fig. 1. On the other hand, the measurement also reveals individual scratches, preferentially aligned along polishing directions, featuring depths of up to 330 nm. Such surface defects are prohibiting large scale optoelectronic applications.

2.2. Polishing mechanism

IBE is a well-known method for microstructuring and surface

* Corresponding authors.
E-mail addresses: sichen.mi@epfl.ch (S. Mi), niels.quack@epfl.ch (N. Quack).

https://doi.org/10.1016/j.diamond.2019.01.007
Received 7 September 2018; Received in revised form 11 January 2019; Accepted 11 January 2019
Available online 16 January 2019

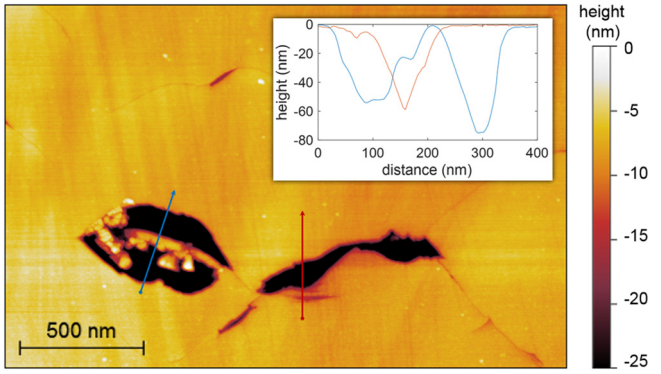

Fig. 1. AFM measurement of mechanically polished SCD substrate. Shallow polishing lines and deep scratches of various morphology are found. The color bar minimum was set to −25 nm to give better visibility for the polishing lines. Inset: height profile along the blue and red lines on the AFM picture, revealing scratch depths of up to 75 nm. The deepest scratch on this particular sample was found to be 330 nm. (For interpretation of the references to color in this figure legend, the reader is referred to the web version of this article.)

smoothening [20,21], in which inert gas ions are accelerated to bombard the material surface, causing curvature dependent erosion and mass redistribution [22] which etch and smoothen the surface at or near normal incidence. Since the material removal is dominated mainly by physical bombardment, IBE is well suited for processing various materials [21]. However, when deep scratches as shown in Fig. 1 are present, which is common after mechanical polishing of brittle materials, conventional IBE schemes are unsuitable for surface polishing because the scratches tend to become exaggerated. In contrast, by taking into consideration the incidence-angle dependent variation of sputtering yield, we show that the IBE process can be configured for the fast removal of these defects.

The ion sputtering yield defined as atoms removed by per incident ion, which is related to both material/ion species and ion beam properties, exhibits incidence-angle dependent behavior [23]. For example, the sputtering yield for 750 eV Ar^+ impinging onto SCD (100) surface at ion beam incidence angle (θ) of 60° is more than five times of that at $\theta = 0°$. More generally, the angle dependent sputtering yield can be described by [23]

$$Y(E,\theta) \propto \frac{E}{UN(2\pi A)^{0.5}} \exp\left(-\frac{\cos^2\theta\alpha^2}{2A}\right) \quad (1)$$

where $A = \cos^2\theta\alpha^2 + \sin^2\theta\beta^2$, with $\alpha(\beta)$ being the energy range straggling along longitudinal(lateral) direction, E the ion energy, a the projected energy range, U the surface binding energy, and N the atomic density. While this formula was originally proposed to describe the angle-dependent sputtering yield for amorphous and polycrystalline materials, empirical data for single crystalline materials show prominent agreement with the model [24], which can be attributed to the ion sputtering induced amorphization. Furthermore, molecular dynamics (MD) simulation on single crystal materials also confirmed good agreement with Eq. (1), although local maxima/minima can be present [25], which, having negligible impact to the process described later, is believed to originate from the crystallographic nature. For certain incidence angles, ions hitting on the sidewall of a pit cause smaller material removal rate (MRR) than on the planar top surface, therefore leading to pit removal in a non-contact way. Here the MRR is calculated taking into consideration flux variation at different incidence angles, based on fitted sputtering yield. For a (100) SCD substrate [24] treated by 750 eV Ar^+, the calculated maximum MRR normalized to that at normal incidence is 2.79, with ion incidence angle in the vicinity of $\theta = 51.2°$ (denoted by θ_m), as illustrated in Fig. 2. Fitting parameters used here are $\alpha = 42.15$, $\beta = 50.37$, and $a = 103.5$. Exact values of other parameters are not relevant since we care only about the normalized results.

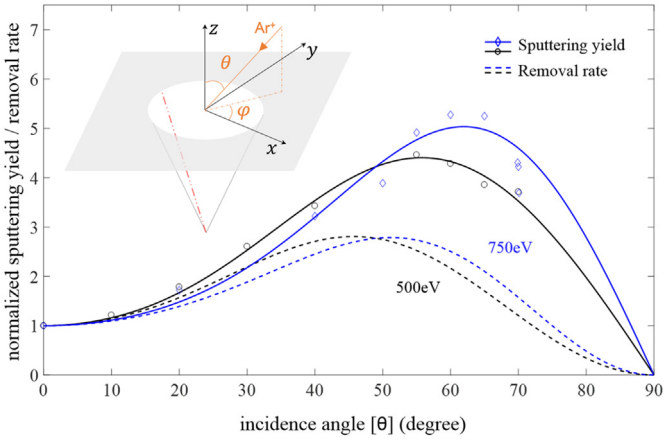

Fig. 2. Angle-dependent sputtering yield and material removal rate normalized to those at normal incidence, based on reference data [24], and fitted with Eq. (1). Inset: schematic of a pit on the planar surface modeled as an inverse cone; θ and φ are polar and azimuthal angle of incident ion beam, respectively; Ar^+ indicates the ion incidence and the red dashed line labels the generatrix of the inverse cone. (For interpretation of the references to color in this figure legend, the reader is referred to the web version of this article.)

2.3. Modeling and simulation

To illustrate the working principle of the process, we model the surface pit as an inverse cone, as shown in Fig. 2, where φ and θ are the azimuthal and polar angle respectively of the incident ion beam. We also define $\chi \equiv r/h$ where r is the base radius and h depth, of the cone, indicating its sharpness. Due to the symmetry, we will only discuss the etching effect on the generatrix marked red in Fig. 2. Without sample rotation during IBE, the pit will gradually become asymmetric; whereas with rotation, as the global incidence angle is kept the same, the sidewall of the pit experiences local incidence angle variation depending on φ, which can give not only an averaged preferential etch on the top surface, but also a dynamical shading effect as long as $\chi < \tan\theta$. This is better illustrated in Fig. 3, where etch rate on the aforementioned generatrix against azimuthal rotation and depth is simulated based on Eq. (1), assuming $\theta = 60°$ and $\chi = 0.4$. The depth is normalized to 1

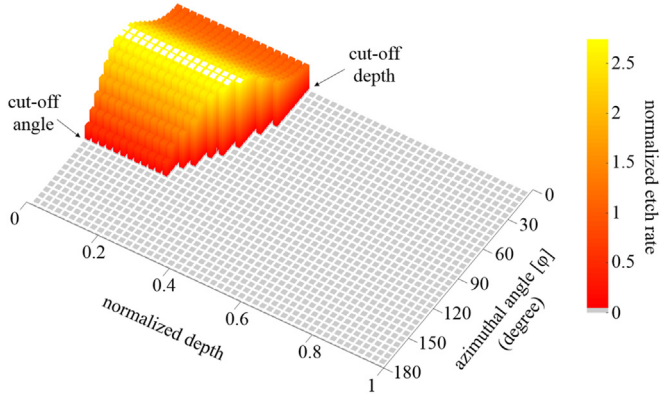

Fig. 3. Etch rate on the generatrix in Fig. 2 as a function of depth and azimuthal rotation, simulated based on Eq. (1), with $\chi = 0.4$ and $\theta = 60°$. Angle-dependence of MRR is calculated according to the blue curve in Fig. 2. Cut-off angle of 103° and cut-off depth of 37.52% at $\varphi = 0°$ are found. The cut-off depth varies with both φ and θ. Beyond cut-off there is no etching at all, as the ion beam is stopped at the planar surface. The model assumes invariance of the inverse cone geometry within one cycle of rotation. As etching continues, the pit shape changes slowly and this diagram will evolve accordingly.

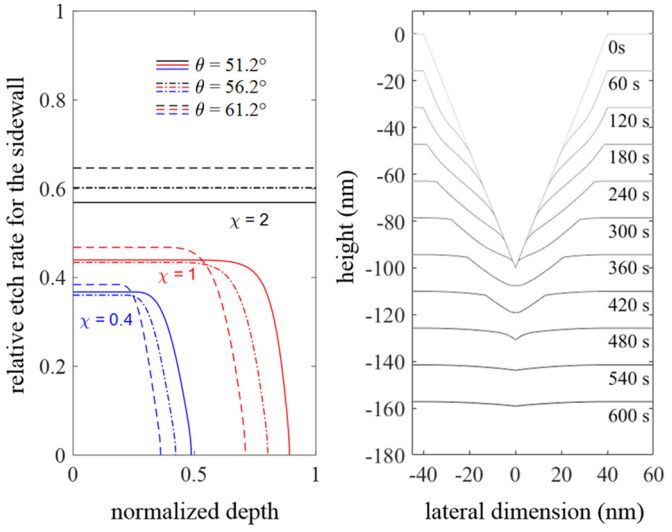

Fig. 4. Left: sidewall etch rate relative to the planar top surface etch rate, averaged over $\varphi \in [0, \pi)$. Cut-off only exists for $\chi < \tan\theta$, and the cut-off depth decreases as θ increases. Best selectivity is found at $\theta > \theta_m$. Right: temporal evolution of the cross-section profile of a pit with $h = 100$ nm and $\chi = 0.4$, simulated based on Eq. (1). Here θ is chosen at 60° and the pit depth is reduced to 2 nm in less than 10 min.

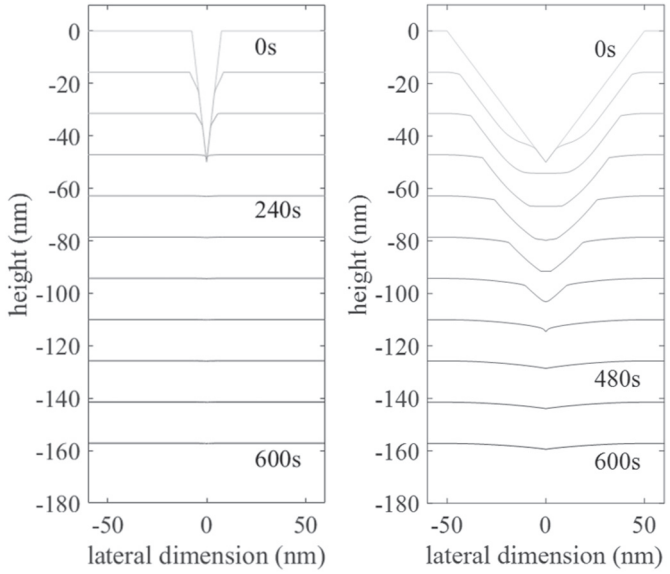

Fig. 5. Temporal evolution of the cross-section profile of a pit with $h = 50$ nm. Here θ is chosen at 60° and the etch rate is set to be experimental data. Narrower pit results in much faster planarization, but the final finish is only slightly better. Left: $\chi = 0.15$. Right: $\chi = 1$.

without loss of generality. The pit geometry is assumed to be invariant during one rotation cycle, which is reasonable as long as the etching rate is not too high, or the rotation speed is not too slow. It is worthwhile to note that the cut-off depth decreases with increasing φ, and no etching occurs for $\varphi > 103°$, due to shading of the ion beam by the planar top surface. Overall, this process manifests a depth dependent etching rate for a surface pit: the averaged MRR on the sidewall keeps at a constant value from $z = 0$ until a certain depth, deeper than which it gradually drops to zero, at the cut-off depth (d_c) at $\varphi = 0°$; for any point deeper than d_c, there is no removal at all. In general, for crystalline materials, material etch rate is also related to crystal plane orientation. However, considering that the IBE process amorphizes the very surface during material removal [26], and that the pit sidewalls do not exhibit well-defined crystalline planes, it is reasonable to assume that this dependence can be neglected. In the case of $\chi > \tan\theta$, only the angle dependence of sputtering yield contributes to material removal. The planar top surface, on the other hand, is always under ion bombardment, regardless of χ, with or without sample rotation.

As shown in Fig. 4, etch rate on the sidewall relative to that on the planar top surface (referred to as selectivity hereafter) at different depth is calculated with varying χ and θ, other parameters being the same as those used for Fig. 3. Similar to MRR, selectivity also keeps at a constant value over certain depth, after which gradually decreases to zero at d_c. However, due to local incidence-angle variation on the sidewall during rotation, best selectivity is not achieved at θ_m: as can be seen for the $\chi = 1$ and $\chi = 0.4$ cases in Fig. 4, a slightly higher θ gives better (smaller) selectivity. For $\chi = 2 > \tan\theta$, no cut-off can be found. To provide a quantitative understanding of the working principle, a 2D axisymmetric simulation was carried out to reveal the cross-section profile evolution in time during IBE treatment with sample rotation. Here the MRR on the planar top surface is set to be about 16 nm/min. In less than 10 min, the pit depth is reduced from 100 nm to 2 nm, for $\chi = 0.4$ and $\theta = 60°$. A comparison between simulations with $\chi = 0.15$ and with $\chi = 1$ is presented in Fig. 5, where smaller χ results in faster planarization and slightly better final finish.

3. Experiment results and discussion

To demonstrate the proposed non-contact polishing method, the SCD substrate shown in Fig. 1 was treated by IBE with sample rotation. In order to monitor individual scratches on the diamond surface, a ten by ten array of square-shaped plateaus is prepared on the substrate, each with 200 nm height and a side-length of 10 μm. The fabrication process is as follows [27,8]: after cleaning of the as-received sample with piranha solution, a silicon dioxide layer is deposited to protect the surface features, also acting as hard mask in subsequent etching; standard photo-lithography is used to pattern and develop spin-coated photo-resist, and the patterns are first transferred to the oxide layer, then to the diamond substrate with two steps of plasma etching, removing the unprotected oxide layer and etching the diamond substrate respectively; finally the hard mask is completely removed by HF etching and the sample is cleaned with piranha once again to remove any residual contamination. Scanning electron microscopy (SEM) examination revealed at least two deep scratches on each plateau. With this arrangement, individual surface scratches were monitored during a 28-minute IBE process with sample rotation at 10 rpm, using a Veeco Nexus IBE350 operating at 700 eV acceleration with Ar^+ ion flux of 1.1 mA/cm^2. The incidence angle was set at 60° instead of θ_m as it gives smaller d_c. The temporal evolution of a single scratch was tracked by SEM before the IBE and after 4, 12, 20 min of treatment, as shown in

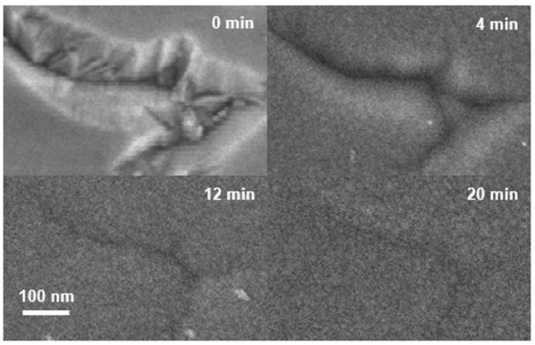

Fig. 6. Temporal evolution of an individual defect recorded by sequential SEM inspection, showing the rapid flattening of a typical defect after 20 min of surface treatment. AFM measurements confirmed reduction of the trench depth from 108 nm to 8 nm in 20 min. By further increasing IBE treatment time, no noticeable change was observed.

Table 1
Depth change of individual surface scratches before and after 28 min of IBE treatment. The measurements reveal increased removal rate for narrower scratches (unit: nm).

Site	Initial width	Initial depth	Finish depth
1	330	140	7
2	196	93	3
3	120	70	3
4	120	66	3
5	250	160	10
6	590	330	40

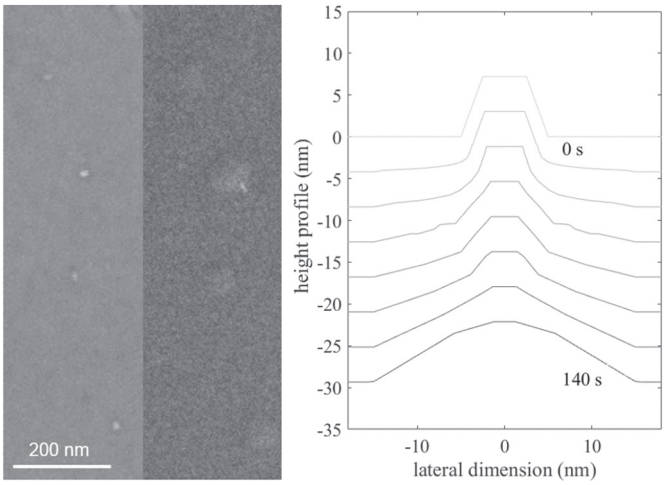

Fig. 7. Left: SEM recording showing nano-sized diamond grits remaining on the SCD substrate after mechanical polishing growing larger after 4 min of IBE treatment with $\theta = 60^{\circ}$. Right: numerical simulation based on Eq. (1) for 140 s predicts growing of initial diamond grits.

Fig. 6. AFM measurement confirmed trench depth reduction from 108 nm to 8 nm in 20 min. Listed in Table 1 are the measurements for other scratches with a variety of initial conditions, where it can be found that the polishing speed experimentally seen is slower than the simulated value for that of the real scratches, for example the ones shown in Fig. 1, do not adopt a perfect inversed-cone shape; besides, it also depends on the effective χ of each defect. Approximately 500 nm diamond layer was removed during this process.

As illustrated by Fig. 4, due to the difference in polishing mechanism, our method needs to etch deeper than the actual depth of the defect to planarize the surface. Nevertheless it is still of similar or much faster polishing speed compared to other fine polishing techniques [28,29]. Moreover, it is possible to accelerate the process linearly just by increasing the ion flux. According to Ref. [30], we estimate the pressure exerted onto the diamond surface to be on the order of 1 Pa in our experiment, six magnitudes smaller than that in Ref. [28,29]. Such mildness is of particular interest in preserving the sub-surface crystalline quality. To give optimal performance, experimental parameters in general can be chosen according to Eq. (1) and empirical data on sputtering yield. Depending on processing purpose and surface characteristics, it is not always optimum to set the incidence angle to θ_m. The selectivity can be tuned by changing the ion acceleration energy and incidence angle, taking into account the pit geometry. In our demonstration, 700 eV was used limited by instrument capabilities, and the IBE treatment with sample rotation nevertheless allowed for rapid removal of deep scratches starting from a variety of initial conditions as listed in Table 1, in spite of the maximum normalized MRR limited to around 2.73. While here we have neglected the nanoscale dynamics such as re-deposition and surface viscous flow [31,22], these phenomena may be explored for self-organized process which we discuss elsewhere [32]. The single-crystalline nature at this scale cannot be simply neglected. Nano-sized roughening however can be easily polished to sub-nanometer level [15] by IBE with small θ, therefore does not limit final finish for this process. By adding oxygen or hydrogen gas into the IBE process, finish quality might be further improved [33,34,16]. One should note that as troughs can be readily removed by preferential etching of the planar top surface, protrudes on the surface tend to grow larger. This is observed in an area where diamond abrasives introduced in mechanical polishing were not completely removed. A comparison before and after 4 min of 60° incidence-angle IBE with sample rotation is shown in Fig. 7. This emphasizes the importance of thorough cleaning before using this method to polish surface, meanwhile indicates as well that 3D structures [35] can be fabricated following the same modeling. A closing remark is that a thin layer of amorphous carbon will be present on the very surface after IBE process, which is estimated to be less than 5 nm by TRIM simulation [36] under our experimental configuration. Such ion beam induced amorphized layer can be readily removed by annealing in air as we have previously demonstrated [27].

4. Conclusions

In summary, we propose and demonstrate a versatile non-contact surface finishing method allowing rapid flattening of surface defects such as scratches and pits on SCD substrates. Based on angle dependent sputtering yield and inert gas ions, this method is applicable to a wide range of existing and emerging material platforms such as gallium nitride, silicon carbide or various ceramics, where the final step of fine polishing typically costs dozens of hours or even more [37]. Since the process proposed relies on physical sputtering, it is a convenient way for surface treatment, without the need to develop specific chemical recipes as usually required in chemical-mechanical polishing and RIE.

Acknowledgments

The authors acknowledge funding by the Swiss National Science Foundation under grant No. 157566. Fabrication and characterization were carried out at the EPFL Center of MicroNanoTechnology (CMi). The authors gratefully acknowledge the support from CMi staff.

References

[1] R. Mildren, J. Rabeau, Optical Engineering of Diamond, John Wiley & Sons, 2013.
[2] A. Ajoy, U. Bissbort, M.D. Lukin, R.L. Walsworth, P. Cappellaro, Atomic-scale nuclear spin imaging using quantum-assisted sensors in diamond, Phys. Rev. X 5 (1) (2015) 011001.
[3] M.J. Burek, C. Meuwly, R.E. Evans, M.K. Bhaskar, A. Sipahigil, S. Meesala, B. Machielse, D.D. Sukachev, C.T. Nguyen, J.L. Pacheco, Fiber-coupled diamond quantum nanophotonic interface, Phys. Rev. Appl. 8 (2) (2017) 024026.
[4] I. Friel, S. Clewes, H. Dhillon, N. Perkins, D. Twitchen, G. Scarsbrook, Control of surface and bulk crystalline quality in single crystal diamond grown by chemical vapour deposition, Diam. Relat. Mater. 18 (5-8) (2009) 808–815.
[5] LakeDiamond, https://www.lakediamond.ch accessed: 2018-08-08.
[6] Element Six, https://www.e6.com accessed: 2018-08-08.
[7] A. Sipahigil, R. Evans, D. Sukachev, M. Burek, J. Borregaard, M. Bhaskar, C. Nguyen, J. Pacheco, H. Atikian, C. Meuwly, et al., An integrated diamond nanophotonics platform for quantum optical networks, Science (2016) aah6875.
[8] A. Toros, M. Kiss, T. Graziosi, H. Sattari, P. Gallo, N. Quack, Precision micro-mechanical components in single crystal diamond by deep reactive ion etching, Microsyst. Nanoeng. 4 (1) (2018) 12.
[9] T. Schuelke, T.A. Grotjohn, Diamond polishing, Diam. Relat. Mater. 32 (2013) 17–26.
[10] Y. Lin, J. Lu, R. Tong, Q. Luo, X. Xu, Surface damage of single-crystal diamond (100) processed based on a sol-gel polishing tool, Diam. Relat. Mater. 83 (2018) 46–53.
[11] N. Yang, W. Zong, Z. Li, T. Sun, Wear process of single crystal diamond affected by sliding velocity and contact pressure in mechanical polishing, Diam. Relat. Mater. 58 (2015) 46–53.
[12] H.A. Atikian, A. Eftekharian, A. Jafari Salim, M.J. Burek, J.T. Choy, A. Hamed Majedi, M. Lončar, Superconducting nanowire single photon detector on diamond, Appl. Phys. Lett. 104 (12) (2014) 122602.
[13] T. Yatsui, W. Nomura, M. Naruse, M. Ohtsu, Realization of an atomically flat surface of diamond using dressed photon-phonon etching, J. Phys. D. Appl. Phys. 45 (47) (2012) 475302.

[14] M. Challier, S. Sonusen, A. Barfuss, D. Rohner, D. Riedel, J. Koelbl, M. Ganzhorn, P. Appel, P. Maletinsky, E. Neu, Advanced fabrication of single-crystal diamond membranes for quantum technologies, Micromachines 9 (4) (2018) 148.
[15] T. Nagase, H. Kato, S. Pahlovy, I. Miyamoto, Nanosmoothing of single crystal diamond chips by 1 keV Ar+ ion bombardment, J. Vac. Sci. Technol., B: Nanotechnol. Microelectron.: Mater., Process., Meas., Phenom. 28 (2) (2010) 263–267.
[16] J. Schmitt, W. Nelissen, U. Wallrabe, F. Völklein, Implementation of smooth nanocrystalline diamond microstructures by combining reactive ion etching and ion beam etching, Diam. Relat. Mater. 79 (2017) 164–172.
[17] N. Tatsumi, K. Harano, T. Ito, H. Sumiya, Polishing mechanism and surface damage analysis of type IIa single crystal diamond processed by mechanical and chemical polishing methods, Diam. Relat. Mater. 63 (2016) 80–85.
[18] A. Kubota, S. Nagae, M. Touge, Improvement of material removal rate of single-crystal diamond by polishing using H_2O_2 solution, Diam. Relat. Mater. 70 (2016) 39–45.
[19] M. Doronin, S. Polyakov, K. Kravchuk, S. Molchanov, A. Lomov, S.Y. Troschiev, S. Terentiev, Limits of single crystal diamond surface mechanical polishing, Diam. Relat. Mater. 87 (2018) 149–155 [Diamond and Related Materials].
[20] W. Liao, Y. Dai, Z. Liu, X. Xie, X. Nie, M. Xu, Detailed subsurface damage measurement and efficient damage-free fabrication of fused silica optics assisted by ion beam sputtering, Opt. Express 24 (4) (2016) 4247–4257.
[21] F. Frost, R. Fechner, B. Ziberi, J. Völlner, D. Flamm, A. Schindler, Large area smoothing of surfaces by ion bombardment: fundamentals and applications, J. Phys. Condens. Matter 21 (22) (2009) 224026.
[22] C.S. Madi, E. Anzenberg, K.F. Ludwig Jr, M.J. Aziz, Mass redistribution causes the structural richness of ion-irradiated surfaces, Phys. Rev. Lett. 106 (6) (2011) 066101.
[23] Q. Wei, K.-D. Li, J. Lian, L. Wang, Angular dependence of sputtering yield of amorphous and polycrystalline materials, J. Phys. D. Appl. Phys. 41 (17) (2008) 172002.
[24] T.J. Whetten, A.A. Armstead, T.A. Grzybowski, A.L. Ruoff, Etching of diamond with argon and oxygen ion beams, J. Vac. Sci. Technol. A 2 (2) (1984) 477–480.
[25] R. Smith, K. Beardmore, Molecular dynamics studies of particle impacts with carbon-based materials, Thin Solid Films 272 (2) (1996) 255–270.
[26] N. Kawasegi, S. Kuroda, N. Morita, K. Nishimura, M. Yamaguchi, N. Takano, Removal and characterization of focused-ion-beam-induced damaged layer on single crystal diamond surface and application to multiple depth patterning, Diam. Relat. Mater. 70 (2016) 159–166.
[27] T. Graziosi, S. Mi, M. Kiss, N. Quack, Single crystal diamond micro-disk resonators by focused ion beam milling, APL Photonics 3 (12) (2018) 126101.
[28] A. Kubota, S. Fukuyama, Y. Ichimori, M. Touge, Surface smoothing of single-crystal diamond (100) substrate by polishing technique, Diam. Relat. Mater. 24 (2012) 59–62.
[29] M. Touge, S. Anan, S. Wada, A. Kubota, Y. Nakanishi, J. Watanabe, Atomic-scale planarization of single crystal diamond substrates by ultraviolet rays assisted machining, Key Engineering Materials, vol. 447, Trans Tech Publ, 2010, pp. 66–70.
[30] T. Trottenberg, A. Spethmann, J. Rutscher, H. Kersten, Non-electrostatic diagnostics for ion beams and sputter effects, Plasma Phys. Controlled Fusion 54 (12) (2012) 124005.
[31] H. Hofsäss, O. Bobes, K. Zhang, Argon ion beam induced surface pattern formation on Si, J. Appl. Phys. 119 (3) (2016) 035302.
[32] S. Mi, C. Santschi, M. Kiss, O.J.F. Martin, N. Quack, Size control of self-organized gold nanoparticles on nanopatterned single crystal diamond, 2018 International Conference on Optical MEMS and Nanophotonics (OMN), 2018, pp. 1–5.
[33] S. Kiyohara, I. Miyamoto, K. Kitazawa, S. Honda, Ion beam assisted chemical etching of single crystal diamond chips, Nucl. Instrum. Methods Phys. Res., Sect. B 121 (1-4) (1997) 510–513.
[34] S. Kiyohara, K. Mori, I. Miyamoto, J. Taniguchi, Oxygen ion beam assisted etching of single crystal diamond chips using reactive oxygen gas, J. Mater. Sci. Mater. Electron. 12 (8) (2001) 477–481.
[35] P. Westerik, W. Vijselaar, J. Berenschot, N. Tas, J. Huskens, J. Gardeniers, Sidewall patterninga new wafer-scale method for accurate patterning of vertical silicon structures, J. Micromech. Microeng. 28 (1) (2017) 015008.
[36] J.F. Ziegler, M.D. Ziegler, J.P. Biersack, SRIM - the stopping and range of ions in matter (2010), Nucl. Instrum. Methods Phys. Res., Sect. B 268 (11-12) (2010) 1818–1823.
[37] H. Aida, H. Takeda, S.-W. Kim, N. Aota, K. Koyama, T. Yamazaki, T. Doi, Evaluation of subsurface damage in GaN substrate induced by mechanical polishing with diamond abrasives, Appl. Surf. Sci. 292 (2014) 531–536.